

Synthesis and Use in Catalysis of Hematite Nanoparticles Obtained from a Polymer Supported Fe(III) Complex

Ambra M. Fiore,^[a] Gaspare Varvaro,^[b] Elisabetta Agostinelli,^[b] Annarosa Mangone,^[c] Elvira De Giglio,^[c] Roberto Terzano,^[d] Ignazio Allegretta,^[d] Maria Michela Dell'Anna,^[a] Saverio Fiore,^{*[e]} and Piero Mastrorilli^{*[a]}

Dedicated to Prof. Rinaldo Poli on occasion of his 65th birthday.

Weakly magnetic hematite (α -Fe₂O₃) nanoparticles were synthesized by heating an amorphous polymer supported iron(III) complex (Fe_POL) at 400 °C for 4 h in air. The growth of nanoparticles (NPs) was studied by PXRD, heating the polymer from 150 °C to 400 °C at 25 °C intervals, revealing that, at all temperatures, the only crystalline phase detected is hematite. Conversely, annealing of Fe_POL at 400 °C for 4 h under nitrogen, yielded a material containing wüstite (FeO) as the

only crystalline phase, supported onto pyrolysed acrylamidic polymer. The synthesized materials were characterized by TXRF, PXRD, SEM-EDS, XPS, Raman and FTIR spectroscopy as well as by magnetic analysis. Differently from natural micrometric hematite, synthesised nano-hematite turned out to be an efficient and recyclable catalyst for the hydrogenation of nitroarenes to the corresponding anilines.

Introduction

In the last few decades, iron oxides minerals received great attention from the scientific community because of their low cost and their abundance in nature.^[1] Among the sixteen known oxides and hydroxides, hematite (α -Fe₂O₃), magnetite (Fe₃O₄), wüstite (FeO) and maghemite (γ -Fe₂O₃) have fundamental scientific and technological importance due to their intrinsic

magnetic properties combined with possible nano dimensional advantage.^[2] Iron oxides nanoparticles (NPs) have applications in several fields such as catalysis,^[3] pigments,^[4] molecular imaging,^[5] wastewater treatment,^[6] phytochemistry^[7] and medicine.^[8] Due to their technological importance, extensive researches have been carried out on the development of various synthetic routes to yield iron oxide nanoparticles with desired properties.^[9] The most common methods for synthesising nanometric iron oxides are chemical co-precipitation,^[10] sol-gel,^[11] hydrothermal method,^[12] solvothermal route,^[13] and microwave assisted hydrothermal techniques.^[14] Among iron oxides, hematite (α -Fe₂O₃) is widely studied and raises great interest for technological applications such as catalysis,^[15] wastewater treatment,^[16] and gas sensors.^[17] It is well known that the shape and size of α -Fe₂O₃ NPs^[18] have a deep impact on their chemical and physical properties such as magnetic^[19] and catalytic applications.^[20]

Back in 1999 the synthesis of nano-sized magnetite and hematite had been reported by thermal treatment of Fe(acac)₃ (acac = acetylacetonate) in 1-propanol.^[21] The authors reported that a small amount of water in the organic solvent drastically influenced the type of iron oxides formed. In fact, by using neat 1-propanol microcrystalline magnetite (Fe₃O₄) formed, while adding 1–3% of water to 1-propanol yielded only hematite (α -Fe₂O₃) which, in turn, slowly transformed into magnetite after a long reaction time. In 2014, Yan et al. synthesized α -Fe₂O₃ nanoparticles by calcination of the spindle-like β -FeOOH precursors at 600 °C for 2 h.^[22] By using co-precipitation method, in 2015 Farahmandjou et al. reported the synthesis of hematite NPs by using FeCl₃·6H₂O as precursor and ammonia solution as precipitator. The α -Fe₂O₃ nano-powders, with a particle size about 30 nm, were obtained by calcination at 500 °C.^[23]

In 2009, Hua et al. reported the procedure for the preparation of α -Fe₂O₃ NPs having dimensions of ca. 80 nm, by

[a] Dr. A. M. Fiore, Prof. M. M. Dell'Anna, Prof. P. Mastrorilli
DICATECh Department
Politecnico di Bari

Via Orabona, 4, 70125 Bari, Italy
E-mail: p.mastrorilli@poliba.it

[b] Dr. G. Varvaro, Dr. E. Agostinelli
Istituto di Struttura della Materia
Consiglio Nazionale delle Ricerche
Research Area Roma 1, Monterotondo Scalo, 00016 Roma, Italy

[c] Prof. A. Mangone, Prof. E. De Giglio
Dipartimento di Chimica
Università degli Studi di Bari-Aldo Moro
Via Orabona, 4, 70125 Bari, Italy

[d] Prof. R. Terzano, Dr. I. Allegretta
Dipartimento di Scienze del Suolo, della Pianta e degli Alimenti
Università degli Studi di Bari-Aldo Moro
Via Amendola, 165/A, 70125 Bari, Italy

[e] Dr. S. Fiore
Institute of Methodologies for Environmental Analysis, National Research Council of Italy (IMAA-CNR)
Tito Scalo, 85050 Potenza, Italy
E-mail: saverio.fiore@cnr.it

Supporting information for this article is available on the WWW under <https://doi.org/10.1002/ejic.202100943>

Part of the "celebratory collection for Rinaldo Poli".

© 2022 The Authors. European Journal of Inorganic Chemistry published by Wiley-VCH GmbH. This is an open access article under the terms of the Creative Commons Attribution Non-Commercial NoDerivs License, which permits use and distribution in any medium, provided the original work is properly cited, the use is non-commercial and no modifications or adaptations are made.

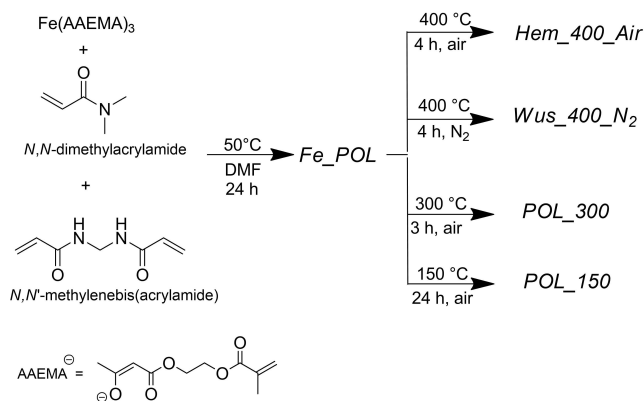
hydrothermal synthesis using FeCl_3 and sodium acetate at 200°C for 12 h.^[24] By using a similar procedure Tadic et al. prepared hematite NPs of size ca. 8 nm, endowed with magnetic properties. These properties were correlated to a combination of magnetically disordered surface shell and magnetically ordered core.^[25]

Many studies have shown how the experimental conditions influence the nature of the synthesized iron oxides.^[26] For example, hematite is the only iron oxide formed by hydrothermal methods at pressures less than 100 bar whereas at pressure higher than 100 bar goethite was formed.^[27]

Herein we describe the synthesis of crystalline nanohematite obtained by heating under air an amorphous polymer supported iron(III) complex and its use in the catalytic hydrogenation of nitroarenes.

Results and Discussion

The starting material for the synthesis of iron oxide nanoparticles was the polymer supported iron(III) complex obtained by copolymerisation of $\text{Fe}(\text{AAEMA})_3$ [AAEMA⁻ = deprotonated form of 2-(acetoacetoxy)ethylmethacrylate] with *N,N'*-meth-



Scheme 1. Synthesis and calcination products of Fe_POL .

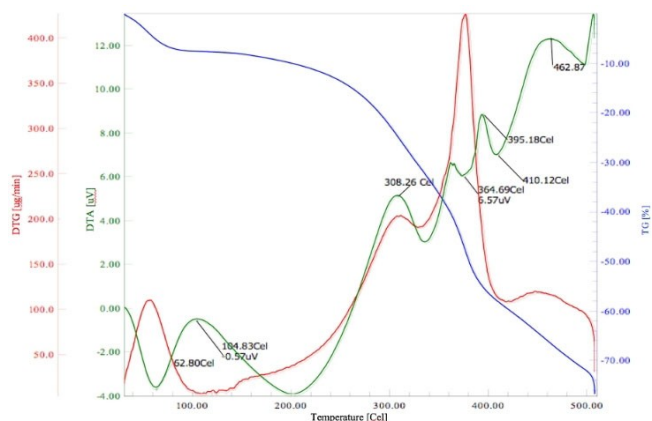


Figure 1. TGA (blue curve), DTG (red curve) and DTA (green curve) of Fe_POL heated under N_2 (rate: $10^\circ/\text{min}$).

ylenebisacrylamide and *N,N*-dimethylacrylamide^[28] and referred to as Fe_POL (Scheme 1).

The thermal behaviour of Fe_POL was studied by TGA/DTA.

Figure 1 shows the TGA, DTG and DTA curves for Fe_POL obtained under N_2 with a heating rate of $10^\circ/\text{min}$.

The thermogravimetric curve (blue line) shows a ca. 9% loss of weight between 25 and 100°C attributable to adsorbed water. Three subsequent steps of weight loss are distinguishable in the ranges $160\text{--}308^\circ\text{C}$, $308\text{--}420^\circ\text{C}$ and $420\text{--}500^\circ\text{C}$; they correspond to 28%, and 58% and 75% weight loss, respectively. The DTA curve shows an endothermic event occurring between 150 and 300°C but no loss of weight. It is plausible that in this temperature interval breaking of C–C bonds resulting in rupture of cross-linkages across the polymer chain takes place.

The relevant loss of weight detected from 308°C to 500°C is due to pyrolysis of the organic matrix of Fe_POL . The three endothermic peaks detected at $308\text{--}364^\circ\text{C}$, $364\text{--}395^\circ\text{C}$, and $395\text{--}462^\circ\text{C}$ may be attributed to the evolution of: CO_2 , NH_3 , H_2O , and N_2 (1st event); amides (acetamide, isobutyramide), cyclic imides, nitriles,^[29] methacrylates and methacrylic acid^[30] (2nd and 3rd events).

In the light of the thermal analysis results, we decided to study the materials obtained by heating Fe_POL at 150°C , 300°C , and 400°C (in the latter case, both under nitrogen and air). The analytical investigations, performed by total reflection X-ray fluorescence (TXRF), FTIR, SEM-EDS, magnetisation curves, indicate that calcination at 150°C and 300°C yielded a composite material constituted by polymer supported iron-based NPs which did not exhibit magnetic behaviour. On the other hand, calcination at 400°C for 4 h in air yielded a material constituted by $\alpha\text{-Fe}_2\text{O}_3$ while, calcination at 400°C for 4 h under N_2 produced a mixture constituted by pyrolysed organic polymer supporting wüstite (FeO) as the only crystalline iron oxide phase.

The dark red powder obtained after Fe_POL heating at 150°C for 24 h (POL_150 , Scheme 1) contained 2.4% of Fe (wt.). The FTIR spectrum (Figure 2) shows intense bands due to C–H, C=O and C–N stretching indicating a structure constituted by an organic polymer supporting iron particles.

The shiny black powder obtained after calcination at 300°C for 3 h in air (POL_300 , Scheme 1) contained 7.5% of Fe and showed, in the $400\text{--}4000\text{ cm}^{-1}$ region, a FTIR spectrum (Figure S1) similar to that of POL_150 . No bands attributable to Fe–O stretching of hematite ($\alpha\text{-Fe}_2\text{O}_3$), maghemite ($\gamma\text{-Fe}_2\text{O}_3$), or magnetite (Fe_3O_4) are observable in the spectrum of POL_150

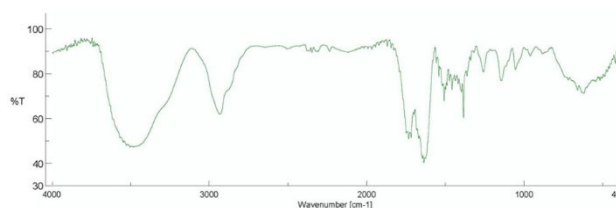


Figure 2. IR (KBr pellet) spectrum of POL_150 .

(Figure 2) whereas two weak bands at about 430 and 500 cm^{-1} are present in the FTIR spectrum of *POL_300* (Figure S1).

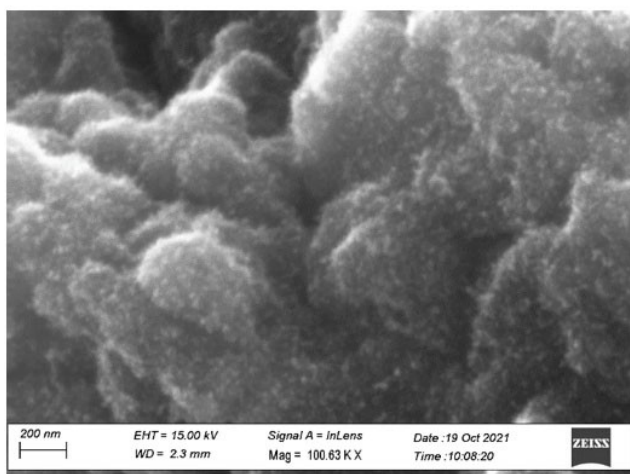
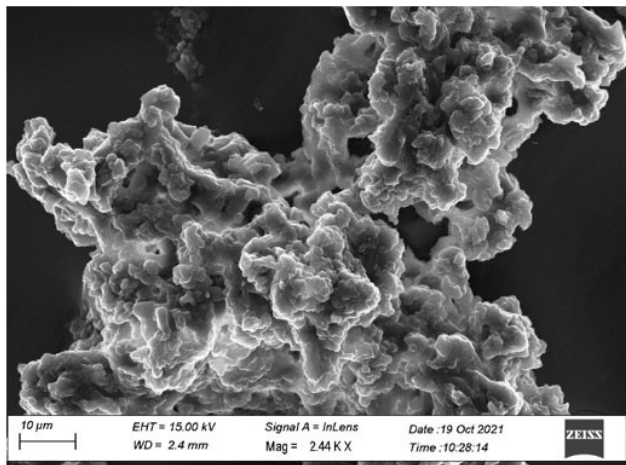


Figure 3. SEM micrographs of *POL_150*.

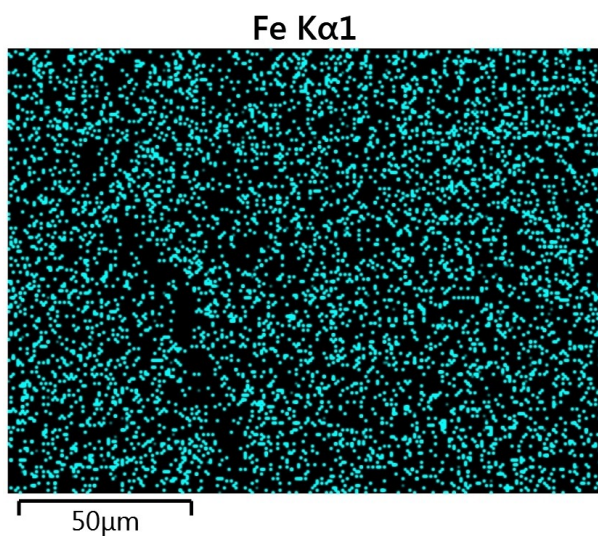


Figure 4. EDS map of *POL_150* showing the Fe distribution onto the polymer.

SEM-EDS analyses of *POL_150* (Figure 3 top) documented that the polymer occurs as microporous grains and it incorporates globular Fe NPs (Figures 3 bottom, and Figure 4).

As for *POL_300*, microscopic observation documented that polymer may occur also as compact grains; Fe NPs are visible on the surface as bumps (Figure 5).

In order to shed light on the formation of crystalline phases in the polymer calcined at 150 or 300 °C we collected the PXRD spectra of *POL_150* and *POL_300*.

POL_150 X-ray diffraction pattern (Figure 6) is characterised by a high background in 2θ interval 2–30°; no peaks attributable to crystalline phases were recorded. The diffraction band centred at 10° 2θ , that disappeared at 300 °C, indicates that the polymer is not amorphous, but its forming molecules are locally ordered probably in microdomains.

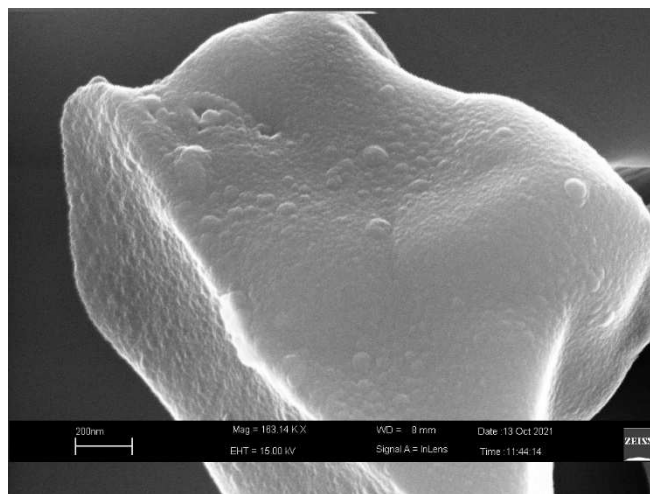


Figure 5. SEM micrograph of *POL_300*.

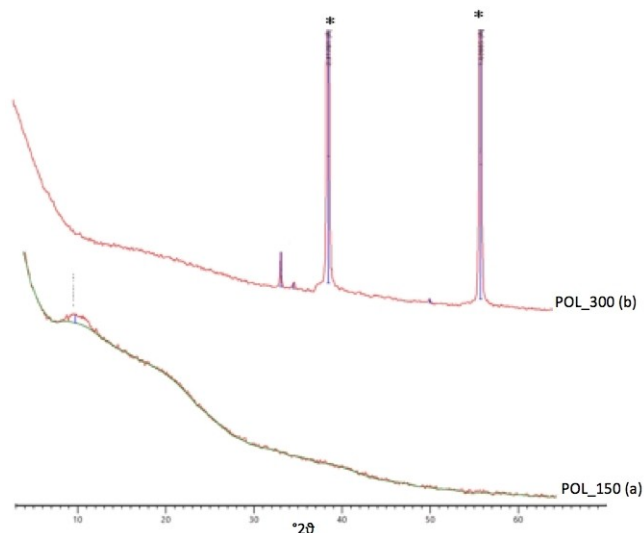


Figure 6. PXRD patterns of *POL_150* (a) and *POL_300* (b). Asterisked peaks refer to NaF.

As for *POL_300*, XRD pattern (Figure 6b) shows peaks at about 33 and $35^\circ 2\theta$ due to $\alpha\text{-Fe}_2\text{O}_3$. The peak at $33^\circ 2\theta$ is strong because of it partially overlaps a NaF line ($33.6^\circ 2\theta$). On the basis of these results, FTIR bands at about 430 and 500 cm^{-1} may be tentatively attributed to the Fe–O stretching of supported hematite.

The red solid obtained after calcination at 400°C for 4 h under air (*Hem_400_Air*, Scheme 1) exhibited a Fe weight percentage of 70.0%: its IR spectrum (Figure 7b) is characterised by intense bands due to Fe–O stretching at 445 and 531 cm^{-1} with only very weak bands attributable to the organic matrix. This indicates that prolonged annealing at 400°C in the air causes the almost complete combustion of the supporting polymer.

The IR spectrum of *Hem_400_Air* is similar but not superimposable to that of natural hematite (*Nat_Hem*, Figure 7a) because of possible difference in particle size^[31] and crystallinity (shift of ca. 20 cm^{-1} in the Fe–O stretching).

The RAMAN spectrum of *Hem_400_Air* (Figure 8) exhibits all the spectral signatures deemed diagnostic for hematite:^[32] two A_{1g} phonon modes (224 and 495 cm^{-1}), four E_g phonon modes

(244 , 291 , 408 and 610 cm^{-1}). Two other bands, at 660 cm^{-1} and the at 1310 cm^{-1} , are also present. A correct assignment of the former is still controversial: some scholars relate it to magnetite or maghemite contamination,^[33] others to the Raman forbidden, IR active longitudinal optical (LO) E_u mode of hematite, activated by disorder within the hematite crystal lattice.^[34] The 1310 cm^{-1} band has been either attributed to a two-magnon scattering, or more recently to an overtone of the previous band, *i.e.* a two-LO phonon scattering process.

A representative SEM picture of *Hem_400_Air* is reported in Figure 9. It can be observed that *Hem_400_Air* mainly consists of subspherical nanoparticles, whose size varied between 6 and 41 nm and having the distribution centred at 21 nm.

The PXRD of *Hem_400_Air* is reported in Figure 10 and reveals that hematite is the only crystalline phase. Scherrer equation analysis carried out on the [104] peak of hematite gave 22.3 nm as average size of the nanoparticles, consistent with SEM observations (mean size = 21 nm, Figure 9).

The formation/transformation of crystalline Fe-phases with temperature was studied in detail by PXRD. Spectra were collected from 150°C to 400°C , at 25°C intervals (Figure S2). Up to 250°C the powder X-ray diffraction analysis confirmed the

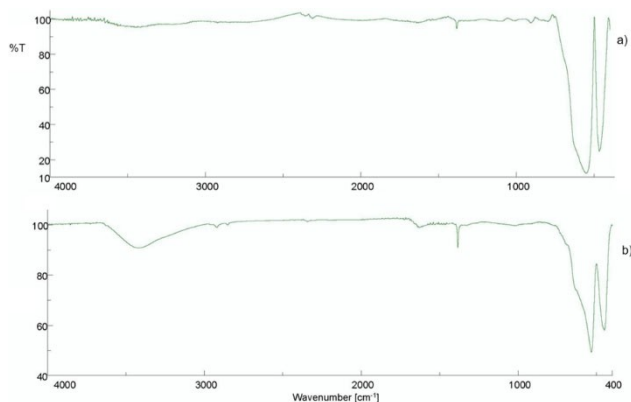


Figure 7. IR spectrum (KBr pellet) of ore hematite (*Nat_Hem*, a) and *Hem_400_Air* (b).

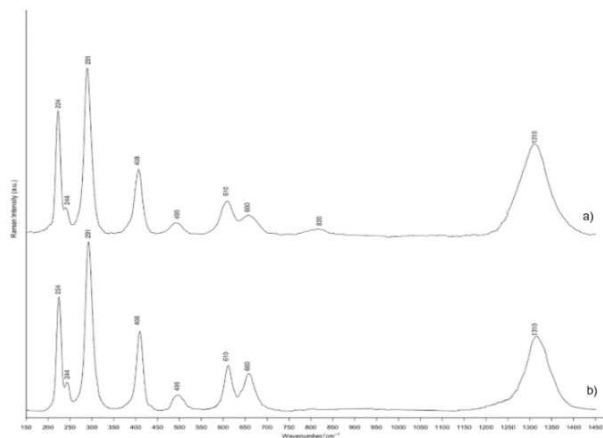


Figure 8. Representative baseline-subtracted Raman spectra acquired with a 633 nm laser –50X LWD objective, 0.6 mW, 3600 s of natural hematite (*Nat_Hem*, a) and *Hem_400_Air* (b).

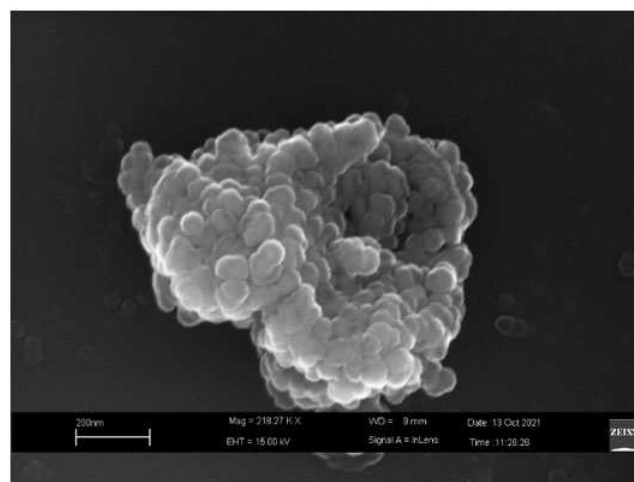


Figure 9. SEM micrograph of *Hem_400_Air* (top) and size distribution of the nanoparticles (bottom).

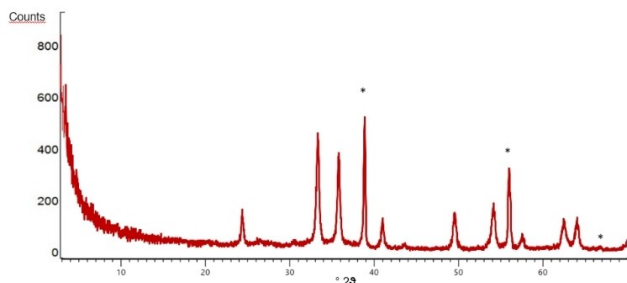


Figure 10. PXRD of *Hem_400_Air*. Asterisked peaks refer to NaF.

presence of the polymer, without any type of crystalline phase. A slight lowering of the background can already be observed at 275–300 °C but the wide hump at 10–22° 2 θ is still present up to 300 °C. At this temperature, the sample shows the presence of some weak lines at 33 and 34° 2 θ , that may be referred to hematite (α -Fe₂O₃). These weak lines become stronger after 325 °C – and even more at 400 °C – and new diffraction lines appear at 34, 27.9 and 41.8° 2 θ thus confirming the crystallisation of hematite. The background flattens out at 350 °C thus indicating the polymer disappearance.

To the best of our knowledge, this is the first experimental evidence of the direct synthesis of nano-hematite by annealing of an amorphous Fe-supported polymer. Iron oxides have been obtained by metal organic deposition from Fe(acac)₃^[35] or from calcination of Fe(acac)₃ at 300, 400 and 500 °C in air, with formation of γ -Fe₂O₃, mixture of γ -Fe₂O₃ and α -Fe₂O₃, α -Fe₂O₃, respectively.^[36]

Given that annealing Fe complexes under inert atmosphere (N₂ or Ar) is known to produce magnetite (Fe₃O₄)^[37] and looking for a method to prepare magnetic iron oxide using a polymeric matrix we annealed *Fe_POL* at 400 °C under N₂.

The shiny black powder obtained (*Wüs_400_N₂*) was shown to be constituted by wüstite (FeO) as the only crystalline phase (Figure 11), supported onto pyrolysed acrylamidic polymer (IR, Figure S3), with a Fe content equal to 22.2%. SEM observations of *Wüs_400_N₂* documented the presence of micrometric rounded grains and shards (Figure S4); high magnifications reveal that they are composed of aggregates of nanoparticles (mean size about 25 nm), as shown in Figure 12. It is interesting to note that annealing *Fe_POL* at 400 °C under N₂ for 0.5 h

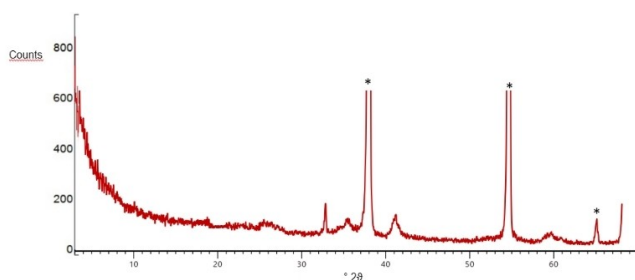


Figure 11. PXRD pattern of *Wüs_400_N₂*.

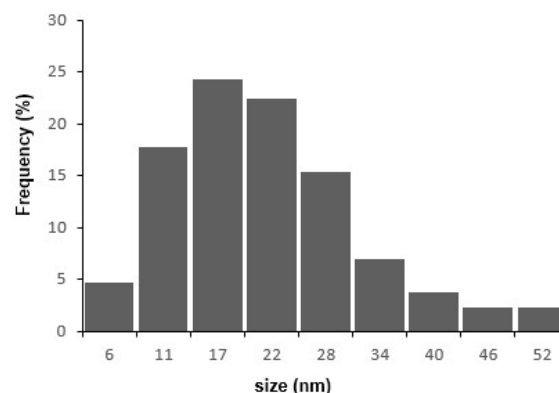
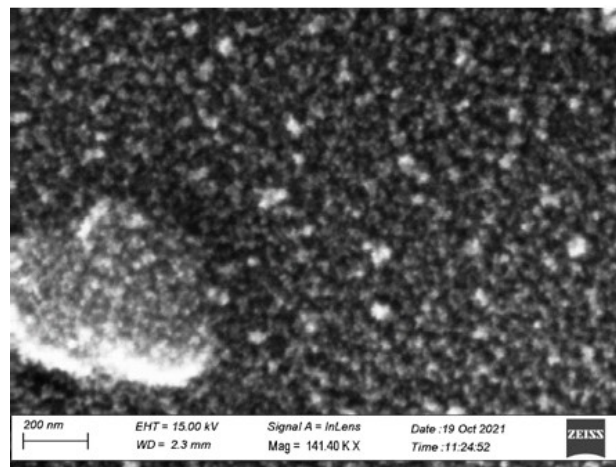


Figure 12. SEM micrograph of *Wüs_400_N₂* (top) and size distribution of the nanoparticles (bottom).

yielded a black material (Fe = 13.5 % wt) containing hematite as the only crystalline phase (Figure S5). This suggests that the transformation of Fe(AAEMA)₃ (initially present onto the polymer) into wüstite can occur via the sequence Fe(AAEMA)₃ → hematite → magnetite → wüstite.

XPS study

XPS analysis has been exploited to examine the surface chemical composition of the investigated materials. In Table 1, the XPS atomic percentages of the elements, detected on *Hem_400_Air* and *Wüs_400_N₂*, are reported. The iron atomic percentages, lower than those expected, could be attributable to the sampling depth of this technique (at most 10 nm) that

Sample	C1s	O1s	Fe2p	Si2p	Na1s	N1s
<i>Hem_400_Air</i>	57.0	31.8	9.4	1.4	0.4	0.1
<i>Wüs_400_N₂</i>	80.5	13.7	0.7	2.0	-	3.2

also reveals an important presence of carbon containing species on the materials surfaces. The almost complete combustion of the polymer in *Hem_400_Air* is confirmed by the negligible amount of found nitrogen on the surface (0.1 atom %), which, in *Wüs_400_N₂*, is expectedly much higher (3.2 atom %). In Figure 13, Fe 2p regions relevant to *Hem_400_Air* (a) and *Wüs_400_N₂* (b) are reported. Previous studies demonstrated that Fe 2p_{3/2} and Fe 2p_{1/2} peak positions depend on the ionic state of the iron but also the satellite peaks have been investigated due to their high sensitivity to the oxidation state. The peak position of Fe 2p_{3/2} for Fe₂O₃-based compounds has been investigated in many studies and values in the range 710.6–711.2 eV have been reported.^[38] Moreover, the satellite peak associated to Fe 2p_{3/2} for Fe₂O₃-based compounds is positioned at values of approximately 8 eV higher than the main Fe 2p_{3/2} peak.^[38,39] In the Fe 2p spectrum of *Hem_400_Air* (Figure 13a), the Fe 2p_{3/2} and Fe 2p_{1/2} binding energies are 710.6 and 724.2 eV, respectively. At 718.7 eV, the satellite peak of the Fe 2p_{3/2} is clearly evident. These data, in agreement with XRD analysis, allowed the attribution of this signal to Fe(III) oxidation state.^[38,40] As far as Fe 2p spectrum of *Wüs_400_N₂* (Figure 13b) is concerned, the binding energies of Fe 2p_{3/2} and Fe 2p_{1/2} are 710.8 and 724.5 eV, respectively. The Fe 2p_{3/2} satellite peak is not clearly evident in this case, but the presence of a weak 'shoulder' satellite peak at

a binding energy difference of about 6 eV seems to confirm the presence of Fe(II) species (indicated by XRD analysis), in agreement with previous literature data.^[38,39b]

Magnetism study

The magnetic behaviour of *Hem_400_Air* and *Wüs_400_N₂* was studied by recording their field-dependent magnetization loops at 300 K (Figure 14) and compared with that of natural hematite. The latter (Figure 14a) shows a finite coercivity ($H_c \sim 0.35$ kOe) and a saturation magnetization ($M_s \sim 4.5$ emu/g), which are lower and larger, respectively, than the values expected for pure bulk hematite (i.e., $H_c = 1\text{--}4$ kOe, $M_s \sim 0.4$ emu/g).^[41] Owing to the micrometre size of the measured natural hematite powder, the observed discrepancy may be related to the presence of magnetite/magnetite impurities (< 5%), which are not detectable by XRD but large enough to affect the magnetic measurements. Synthesized particles (Figures 14b and 14c) present an almost zero remanence and coercivity, thus suggesting that the nanoparticles are close to the superparamagnetic regime owing to their reduced size. The magnetization value corresponding to the maximum available field (2 T), M^{2T} , of the *Hem_400_Air* sample is significantly larger

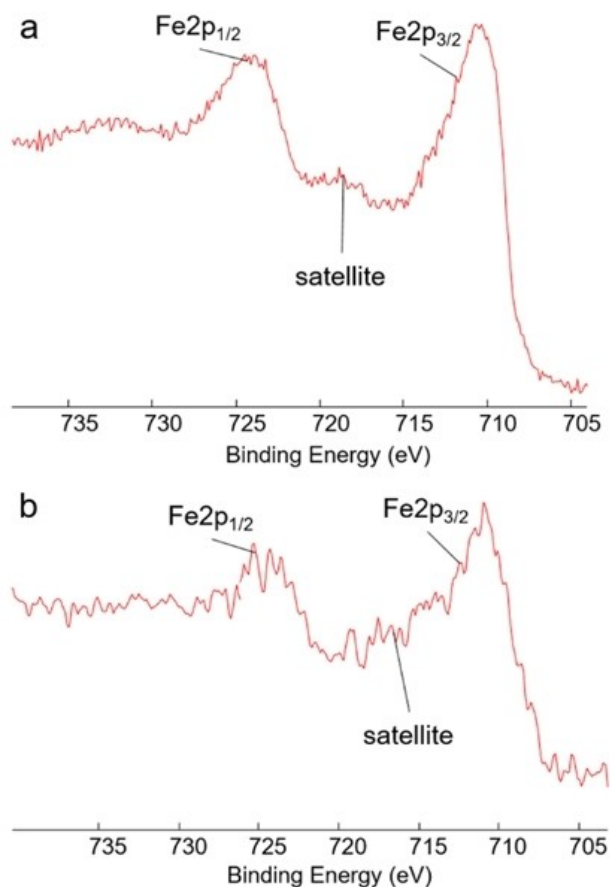


Figure 13. XPS Fe2p signals recorded on *Hem_400_Air* (a) and *Wüs_400_N₂* (b).

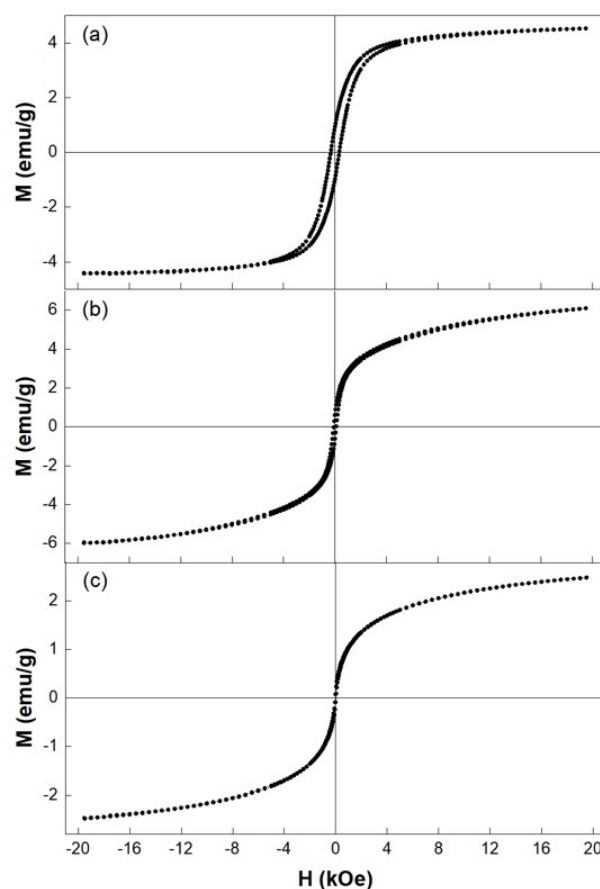


Figure 14. Normalized magnetization loops measured at 300 K of: *Hem_400_Air* (a); *Wüs_400_N₂* (b); ore hematite *Nat_Hem* (c).

that the bulk hematite value and may be ascribed to traces of maghemite and/or magnetite and/or surface spin disorder.^[25] The field-dependent magnetization loop of the *Wüs_400_N2* sample is compatible with wüstite nanoparticles with uncompensated surface spins,^[42] even if the presence of traces of other Fe oxide phases cannot be excluded.

Catalytic tests

Recently, iron oxide-based catalysts for selective hydrogenation of nitroarenes to anilines^[43] have aroused much interest^[44] for economic and sustainability related reasons, being iron an earth abundant metal. Among iron(III) oxides, the well-known active catalyst for this reaction is γ -Fe₂O₃.^[45] To date, the use of nano-hematite as catalyst for the hydrogenation of nitroarene has been only seldom described^[46] and, in any case, nano-structured α -Fe₂O₃ has been demonstrated to be less active than γ -Fe₂O₃ and Fe₃O₄ nanoparticles under hydrogen pressure (30 bar) at 150 °C.^[47] Negligible activity of pure (not nanometric) α -Fe₂O₃ in nitroarene reduction has been reported by Dong^[48] when hydrazine hydrate was used as the reductant.

Preliminary catalytic tests were carried out using *Hem_400_Air* as catalyst and nitrobenzene as substrate. Results are reported in Table S1. By employing NaBH₄ as reducing agent and ethanol as solvent, the yield into aniline was negligible both at room temperature (entries 1 and 2 in Table S1) and at reflux (entry 3). By using neat water as solvent, the yield slightly increased (27% after 3 h and 30% after 12 h, entries 4 and 5, respectively). Increasing the NaBH₄/substrate molar ratio up to 20 did not improve the catalytic performance (entry 6). Poor yields were obtained either by using EtOH/H₂O as mixed solvent (entry 7), or by using hydrazine monohydrate (N₂H₄·H₂O) as a reducing agent at room temperature in EtOH (entries 8–9). Maintaining these experimental conditions but raising the temperature to ca. 80 °C (refluxing ethanol) permitted to achieve a quantitative yield in aniline after 3 h reaction (entry 10).

Once optimized the experimental conditions for the hydrogenation of nitrobenzene to aniline, the best synthetic procedure (N₂H₄·H₂O in EtOH at reflux) was applied for the hydrogenation of *p*-bromonitrobenzene using *Hem_400_Air* (consisting of nano-hematite) and *POL_300* (consisting of acrylamidic polymer supporting hematite) as catalysts. Results are collected in Table 2. While quantitative yield in *p*-bromoaniline was achieved using *Hem_400_Air* after 3 h reaction (entry 1), the yields obtained with *POL_300* were unsatisfactory: 20% after 3 h (entry 2), 25% after 6 h (entry 3) and 40% after 6 h but with a 20-fold excess of N₂H₄·H₂O (entry 4). A possible explanation of the poor catalytic activity observed for *POL_300* could reside in its morphology, which appeared not properly nanostructured as for *Hem_400_Air*, with consequent detrimental effect for the catalysis. In addition, it is widely recognized that the supporting organic matrix plays a key (positive or negative) role in the whole catalytic cycle.^[49] In this case, the presence of organic residues might hamper the migration of the substrates towards the catalytic centres, thus lowering the

Table 2. Hydrogenation of *p*-bromonitrobenzene catalysed by *Hem_400_Air*, *POL_300* or natural hematite.

Entry ^[a]	Catalyst	Reaction time	N ₂ H ₄ ·H ₂ O/ <i>p</i> -BrPhNO ₂ molar ratio	Yield ^[b]
1	<i>Hem_400_Air</i>	3	10	> 99
2	<i>POL_300</i>	3	10	20
3	"	6	10	25
4	"	6	20	40
5	<i>Nat_Hem</i>	3	10	2

[a] Reaction conditions: 0.50 mmol of *p*-bromonitrobenzene; Fe/substrate molar ratio = 0.18. [b] Yield determined by GLC with the internal standard method.

final yields, as already observed, for example, for ceria-based nanocomposites.^[50]

Since the nanometric hematite in *Hem_400_Air* turned out to be an efficient and selective catalyst for the hydrogenation of nitrobenzene and *p*-bromonitrobenzene, the question arises whether ore hematite is also an active catalyst for this reaction. Thus, we tested natural micrometric hematite (*Nat_Hem*) in the hydrogenation of *p*-bromonitrobenzene. After 3 h, negligible yield in *p*-bromonitroaniline was obtained (entry 5), confirming results reported by Dong.^[48] The difference in catalytic performance between natural hematite and *Hem_400_Air* may then be ascribed to the particle size and shape: nanometric spheres in *Hem_400_Air*, micrometric plates in natural hematite (Figure S7).

The recyclability of the weakly magnetic *Hem_400_Air* was tested by using the same catalyst, recovered with a magnet, in five subsequent reactions of hydrogenation of *p*-bromonitrobenzene. As shown in Figure 15, the recycled *Hem_400_Air* kept intact its activity and selectivity for at least five cycles.

Finally, *Hem_400_Air* was employed in the hydrogenation of the nitrobenzenes X-Ph-NO₂ with X=Cl, I, OH, F, CH₃, OCH₃ (Table 3). Excellent yield in the corresponding substituted anilines was achieved with *p*-chloronitrobenzene (entry 2) and

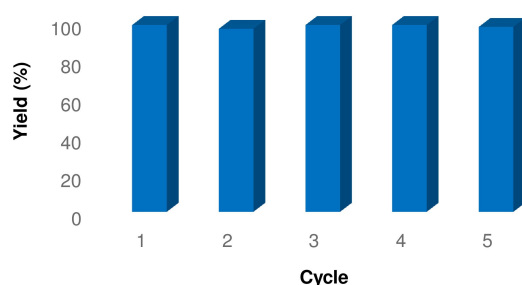


Figure 15. Recyclability of *Hem_400_Air* in the hydrogenation of *p*-bromonitrobenzene to *p*-bromoaniline. In each run the reaction conditions were: 0.50 mmol of *p*-bromonitrobenzene; Fe/substrate molar ratio = 0.18; N₂H₄·H₂O/*p*-bromonitrobenzene molar ratio = 10; solvent and temperature = refluxing ethanol; time = 3 h.

p-nitrophenol (entry 3), while a high yield of 88% was obtained with *p*-iodonitrobenzene (entry 4), due to a little extent of hydrodehalogenation. Higher degree of hydrodehalogenation is held responsible for the 78% yield obtained with *p*-fluoronitrobenzene (entry 5). High yield in the corresponding anilines was achieved with *p*-nitrotoluene (entry 6) and *p*-methoxynitrobenzene (entry 7). The hydrogenation of nitroarenes can follow two pathways that is direct and condensation routes.^[44b] The direct route gives the aniline product through the formation of nitrosoarene and phenylhydroxylamine intermediates. In the condensation route, nitrosoarene and phenylhydroxylamine react to give azoxyarene and azoarene intermediates prior to aniline formation.^[51] Since azoderivates intermediates were never detected while monitoring the reactions catalysed by nanohematite, we favour direct route as operative, as already reported for analogous iron based systems.^[45d,52]

Conclusion

Annealing of the polymer supported iron(III) complex *Fe_POL* resulted in a partial or complete loss of the polymeric support, depending on the reaction conditions. When annealing was carried out in air, crystalline nano-hematite (*Hem_400_Air*) with mean size of nanoparticles of 21 nm was produced. *Hem_400_Air* turned out to be an active, selective, and recyclable catalyst for the transfer hydrogenation of nitroarenes to anilines, a feature likely associated to the nanometric dimension of the synthesised hematite, as micrometric (natural) hematite turned out to be almost inactive. The performance of nano-structured hematite in transfer hydrogenation catalysis is not inferior to that of maghemite or magnetite, the oxides most frequently used in this reaction. Annealing carried out under inert atmosphere yielded pyrolysed acrylamidic polymer supported wüstite (*Wüs_400_N₂*). Both *Hem_400_Air* and *Wüs_400_N₂* showed weak magnetic properties which may ascribed to the presence of hematite and wüstite nanoparticles, respectively, with a surface spin disorder. The presence of magnetite/maghemite impurities cannot be excluded.

Experimental Section

Fe(AAEMA)₃^[28] was obtained as reported in literature. The copolymer of Fe(AAEMA)₃ (*Fe_POL*) was obtained by thermal copolymerization of the AAEMA complexes with *N,N*-dimethylacrylamide and *N,N*-methylenebisacrylamide in *N,N*-dimethylformamide, following the procedure reported in literature.^[53] Micaceous hematite (herein referred to as *Nat_Hem*) comes from Elba Island (Italy). All other chemicals were purchased from commercial providers and used as received. Iron content in all Fe containing materials was assessed by total-reflection x-ray fluorescence (TXRF) spectroscopy, using a S2Picofox spectrometer (Bruker GmbH, Germany) equipped with a Mo source (50 kV and 600 μ A), a multilayer monochromator and a XFlash[®] SDD detector with an active area of 30 mm² (energy resolution < 150 eV@Mn- $K\alpha$). For the analysis, Ga was added as internal standard at a final concentration of 1.0 mg/L. Then, 10 μ L of the prepared solution were deposited on a quartz reflector and

Table 3. Hydrogenation of substituted nitrobenzenes catalysed by *Hem_400_Air*.

Entry ^[a]	X	Yield ^[b]
1	H	> 99
2	Cl	98
3	OH	97
4	I	88
5	F	78
6	CH ₃	90
7	OCH ₃	85

[a] Reaction conditions: 0.50 mmol of substrate; Fe/substrate molar ratio = 0.18; N₂H₄·H₂O/substrate molar ratio = 10; reaction time = 3 h. [b] Yield determined by GLC with the internal standard method.

left drying on a hot plate at 50 °C. Samples were analysed for 1000 s (live time). The samples for TXRF analysis were preliminarily subjected to microwave irradiation with an ETHOS E-TOUCH Milestone applicator, after addition of HCl/HNO₃ (3:1 v/v) solution (12 mL) to each weighted sample. Microwave irradiation up to 1000 W was used, the temperature being ramped from rt to 220 °C in 10 min and the sample being held at this temperature for 10 min. After cooling to room temperature, the digested Fe samples was diluted to 1000 mL before submitting to TXRF analysis. Thermogravimetric analyses were performed using a Hitachi STA 7200, fluxed with nitrogen (80 mL/min) in the range 25–500 °C with a heating rate of 10 °C/min. PXRD investigations were performed using Cu radiation by an X'Pert PANalytical equipped with X-Celerator detector, and by a Rigaku (Japan) MiniFlex2. Since the amount of synthesised material was not sufficient for filling in the sample holder for PXRD analyses, villiumite (NaF) has been used as "support". GC-MS data (EI, 70 eV) were acquired on a HP 6890 instrument using a HP-5MS cross-linked 5% phenylmethylsiloxane (30.0 m × 0.25 mm × 0.25 μ m) capillary column coupled with a mass spectrometer HP 5973. The products were identified by comparison of their GC-MS features with those of authentic samples. FT-IR spectra (in KBr pellets) were recorded on a Jasco FT-IR 4200 spectrophotometer. SEM-EDS observations and analyses were performed using a Field Emission Gun - Scanning Electron Microscope (Zeiss, SUPRA 40) equipped with an Energy Dispersive X-ray Spectrometer (EDS, Oxford Inca Energy 350). XPS analyses were performed on a scanning microprobe PHI 5000 VersaProbe II, purchased from Physical Electronics (Chanhassen, MN). The instrument is equipped with a micro-focused monochromatized AlK α X-ray radiation source. The samples were examined in HP mode with an X-ray take-off angle of 45° (instrument base pressure ca. 10⁻⁹ mbar). The size of the scanned area was about 1400 × 200 μ m. Wide scans and high-resolution spectra were recorded in FAT mode for each sample, setting pass energy values equal to 117.4 eV and 29.35 eV, respectively. Atomic percentages were inferred from peak areas, previously normalized by MultiPak library's sensitivity factors. Adventitious carbon C1s was set as reference charge (284.8 eV). RAMAN investigations were carried out employing LabRAMHR Evolution[®] (Horiba[®], Kyoto, Japan) spectrometer, equipped with a Peltier-cooled charge-coupled device detector (CCD), a He-Ne 633 nm lasers, a BH2[®] microscope (Olympus Corporation[®], Tokyo, Japan). The used parameters were adjusted after several tests finding a compromise between intensity, noise abatement and performance; the laser power was always kept below 0.7 mW at the sample, to avoid sample degradation. After each spectrum had

been recorded, a careful visual inspection was performed using white light illumination on the microscope stage to detect any change that could have been caused by the laser. System has been calibrated using the 520.7 cm^{-1} Raman band of silicon before each experimental session. A 50X long-working-distance (Olympus, Tokyo, Japan, N.A. 0.50) objective was used. The spectral resolution achieved with the 1800 g/mm grating was of about 1 cm^{-1} . A linear baseline was subtracted from the raw spectra using the software LabSpec6® (Horiba®, Kyoto, Japan). Substances were identified by the comparison with reference spectra of minerals. The magnetic behaviour of the annealed materials was preliminarily ascertained by checking whether a neodymium magnet was able to attract the powders. For samples exhibiting magnetic behaviour (*Hem_400_Air*, *Wüs_400_N₂*) magnetisation curves were recorded. For samples exhibiting magnetic behaviour (*Hem_400_Air*, *Wüs_400_N₂*) field-dependent magnetisation loops were recorded at room temperature by using a commercial vibrating sample magnetometer (MicroSense Model 10) with a maximum magnetic field of 2 T.

Synthesis of iron oxide materials

POL_150

Solid *Fe_POL* (2.0 g) was annealed in air at 150 °C for 24 h, yielding a deep red solid referred to as *POL_150*. Yield: 1.8 g. TXRF: Fe 2.40%. IR (cm^{-1}): 3482, 2930, 2874, 1727, 1625, 1498, 1449, 1383, 1257, 1144, 1103, 1053, 958, 878.

POL_300

Solid *Fe_POL* (1.0 g) was annealed in air at 300 °C for 3 h under air, yielding a black powder referred to as *POL_300*. Yield: 0.500 g. TXRF: Fe 7.47%. IR (cm^{-1}): 3475, 2927, 2874, 1721, 1627, 1496, 1449, 1402, 1355, 1255, 1209, 1142, 1104, 1051, 934. 745, 626

Hem_400_Air

Solid *Fe_POL* (1.5 g) was annealed in air at 400 °C for 4 h, yielding a red powder referred to as *Hem_400_Air*. Yield: 0.050 g. TXRF: Fe 70.0%. IR (cm^{-1}): 3421, 1629, 1382, 531, 445. RAMAN: 224, 244, 291, 408, 495, 610, 1310 cm^{-1} .

Wüs_400_N₂

Solid *Fe_POL* (0.780 g) was annealed under nitrogen at 400 °C for 4 h, yielding a black shiny powder referred to as *Wüs_400_N₂*. Yield: 0.080 g. TXRF: Fe 22.2%. IR (cm^{-1}): 3420, 2918, 2863, 1645, 1599, 1435, 1264 (sh), 750, 574, 420.

General experimental procedure for the reduction of nitroarenes catalyzed by hematite nanoparticles

0.50 mmol of nitroarene, 7.0 mg of *Hem-400_Air* ($\text{Fe}\%_{\text{w}}=70$, 0.09 mmol of Fe) and 5.0 mmol of hydrazine monohydrate were stirred at reflux in 5 mL of ethanol for 3 h. The progress of the reaction was monitored by GC-MS. The organic phase was removed, and the catalyst washed several times with ethanol and diethyl ether to remove any traces of organic material. The final product was concentrated under reduced pressure to yield the crude product, which was characterized by GC-MS by comparison with authentic samples.

Recycling experiments

At the end of reaction, the organic layer was removed with a syringe and the catalyst was washed with ethanol and diethyl ether ($3\times 5\text{ mL}$), and then, added of fresh reagents. Iteration of this procedure was repeated for five reuses of the catalytic system.

Author statement

AMF conceived the idea, carried out PXRD, TGA-DTA, FTIR analyses and contributing heavily to editing. GV and EA investigated the magnetic properties and contributed to editing. AM carried out Raman analysis and contributed to editing. EDG carried out XPS analysis and contributed to editing. RT and IA carried out TXRF, some XRD analysis and contributed to editing. MMD conceived the idea and contributing to editing. SF contributed to editing. PM wrote the paper.

Acknowledgements

A.M.F. is indebted to Department of Earth and Geoenvironmental Sciences (University of Bari, Italy) for having made PXRD and TGA-DTA apparatus available for the analytical measurements. Thanks to Dr. Antonio Lettino (IMAA-CNR, Potenza, Italy) and Mr. Adriano Boghetich (DICATECh, Polytechnic University of Bari, Italy) for their help for SEM-EDS observations. Open Access Funding provided by Politecnico di Bari within the CRUI-CARE Agreement.

Conflict of Interest

The authors declare no conflict of interest.

Data Availability Statement

Research data are not shared.

Keywords: Hematite nanoparticles · Heterogeneous catalysis · Magnetic properties · Nitroarenes · Transfer hydrogenation

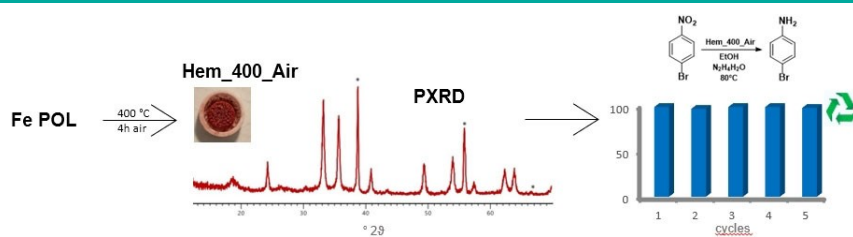
- [1] a) R. M. Cornell, U. Schwertmann, *The Iron Oxides*, Wiley-VCH Weinheim 2003; b) G. S. Parkinson, *Surf. Sci. Rep.* 2016, 71, 272–365.
- [2] a) N. Ajinkya, X. Yu, P. Kaithal, H. Luo, P. Somani, S. Ramakrishna, *Materials* 2020, 13, 4644; b) J. Mondal, K. T. Nguyen, A. Jana, K. Kurniawan, P. Borah, Y. Zhao, A. Bhaumik, *Chem. Commun.* 2014, 50, 12095–12097; c) S. Laurent, D. Forge, M. Port, A. Roch, C. Robic, L. Vander Elst, R. N. Muller, *Chem. Rev.* 2008, 108, 2064–2110.
- [3] a) H. He, Y. Zhong, X. Liang, W. Tan, J. Zhu, C. Y. Wang, *Sci. Rep.* 2015, 5, 10139; b) R. V. Jagadeesh, A. E. Surkus, H. Junge, M. M. Pohl, J. Radnik, J. Rabeah, H. Huan, V. Schunemann, A. Bruckner, M. Beller, *Science* 2013, 342, 1583–1587; c) P. D. Stevens, J. Fan, H. M. R. Gardimalla, M. Yen, Y. Gao, *Org. Lett.* 2005, 7, 2085–2088; d) Z. Zhong, J. Teo, M. Lin, J. Ho, *Top. Catal.* 2008, 49, 216–226.
- [4] J. Wang, W. B. White, J. H. Adair, *J. Am. Ceram. Soc.* 2005, 88, 3449–3454.
- [5] a) J. Wallyn, N. Anton, T. F. Vandamme, *Pharmaceutica* 2019, 11, 601; b) P. Oswald, O. Clement, C. Chambon, E. Schouman-Claeys, G. Frijja, *Magn. Reson. Imaging* 1997, 15, 1025–1031; c) F. Hu, L. Wei, Z. Zhou, Y. Ran, Z. Li, M. Y. Gao, *Adv. Mater.* 2006, 18, 2553–2556.

- [6] M. Kumari, C. U. Pittman, D. Mohan, *J. Colloid Interface Sci.* **2015**, *442*, 120–132.
- [7] R. Alex, N. Sreeju, P. Daizy, *RSC Adv.* **2016**, *6*, 94206–94217.
- [8] S. Mornet, S. Vasseur, F. Grasset, P. Veverka, G. Goglio, A. Demourgues, J. Portier, E. Pollert, E. Duguet, *Prog. Solid State Chem.* **2006**, *34*, 237–247.
- [9] a) U. Schwertmann, R. M. Cornell, *Iron Oxides in the Laboratory*, Wiley-VCH Weinheim **2000**; b) A. G. Roca, L. Gutiérrez, H. Gavilán, M. E. Fortes Brollo, S. Veintemillas-Verdaguer, M. del Puerto Morales, *Adv. Drug Delivery Rev.* **2019**, *138*, 68–104.
- [10] a) T. Xia, J. Wang, C. Wu, F. Meng, Z. Shi, J. Lian, J. Feng, J. Meng, *CrystEngComm* **2012**, *14*, 5741–5744; b) C. Pereira, A. M. Pereira, M. Rocha, C. Freire, C. F. G. C. Geraldes, *J. Mater. Chem. B* **2015**, *3*, 6261–6273; c) K. Petcharoen, A. Sirivat, *Mater. Sci. Eng. C* **2012**, *177*, 421–427.
- [11] a) S. Mishra, E. Jeanneau, M. Rolland, S. Daniele, *Nanomaterials RSC Adv.* **2016**, *6*, 1738–1743; b) J. Xu, H. Yang, W. Fu, K. Du, Y. Sui, J. Chen, Y. Zeng, M. Li, G. Zou, *J. Magn. Mater.* **2007**, *309*, 307–311.
- [12] a) P. Nadoll, T. Angerer, J. L. Mauk, D. French, J. Walshe, *Ore Geol. Rev.* **2014**, *61*, 1–32; b) M. Mohammadikish, *Ceram. Int.* **2014**, *40*, 1351–1358.
- [13] a) J. Park, K. An, Y. Hwang, J. G. Park, H. J. Noh, J. Y. Kim, J. H. Park, N. M. Hwang, T. Hyeon, *Nat. Mater.* **2004**, *3*, 891–895; b) Y. Hou, J. Yu, S. Gao, *J. Mater. Chem.* **2003**, *13*, 1983–1987; c) Z. Xu, C. Shen, Y. Hou, H. Gao, S. Sun, *Chem. Mater.* **2009**, *21*, 1778–1780.
- [14] a) A. Rizzuti, M. Dassisi, P. Mastrorilli, M. C. Sportelli, N. Cioffi, R. A. Picca, E. Agostinelli, G. Varvaro, R. Caliendo, *J. Nanopart. Res.* **2015**, *17*, 408; b) X. Li, D. Liu, S. Song, X. Wang, X. Ge, H. Zhang, *CrystEngComm* **2011**, *13*, 6017–6020.
- [15] a) B. Ahmmad, K. Leonard, S. Islam, J. Kurawaki, M. Muruganandham, T. Ohkubo, Y. Kuroda, *Adv. Powder Technol.* **2013**, *24*, 160–167; b) A. K. Patra, A. Dutta, A. Bhaumik, *Chem. Eur. J.* **2013**, *19*, 12388–12395; c) H. Nagabhushana, S. S. Saundalkar, L. Muralidhar, B. M. Nagabhushana, C. R. Giriya, D. Nagaraja, M. A. Pasha, V. P. Jayashankara, *Chin. Chem. Lett.* **2011**, *22*, 143–146.
- [16] a) V. A. Grover, J. Hu, K. E. Engates, H. J. Shipley, *Nanomater. Environ.* **2012**, *31*, 86–92; b) B.-H. Jeon, B. A. Dempsey, W. D. Burgos, R. A. Royer, *Water Res.* **2003**, *37*, 4135–4142.
- [17] X. L. Fang, C. Chen, M. S. Jin, Q. Kuang, Z. X. Xie, S. Y. Xie, R. B. Huang, L. S. Zheng, *J. Mater. Chem.* **2009**, *19*, 6154–6160.
- [18] A. Lassoued, B. Dkhil, A. Gadri, S. Ammar, *Results Phys.* **2017**, *7*, 3007–3015.
- [19] a) R. D. Zysler, D. Fiorani, A. M. Testa, L. Suber, E. Agostinelli, M. Godinho, *Phys. Rev. B* **2003**, *68*, 212408–1–4; b) L. Liu, H. Z. Kou, W. Mo, H. Liu, Y. Wang, *J. Phys. Chem. B* **2006**, *110*, 15218–15223.
- [20] a) G. H. Wang, W. C. Li, K. M. Jia, B. Spliethoff, F. Schuth, A. H. Lu, *Appl. Catal. A* **2009**, *364*, 42–47; b) Y. Zheng, Y. Cheng, Y. Wang, F. Bao, L. Zhou, X. Wie, Y. Zhang, Q. Zheng, *J. Phys. Chem. B* **2006**, *110*, 3093–3097.
- [21] H. Kominami, S. Onoue, K. Matsuo, Y. Kera, *J. Am. Ceram. Soc.* **1999**, *82*, 1973–1940.
- [22] H. Yan, X. Su, C. Yang, J. Wang, C. Niu, *Ceram. Int.* **2014**, *40*, 1729–1733.
- [23] M. Farahmandjou, F. Soflaee, *Phys. Chem. Res.* **2015**, *3*, 191–196.
- [24] J. Hua, J. Gengsheng, *Mater. Lett.* **2009**, *63*, 2725–2727.
- [25] M. Tadic, M. Panjan, V. Damnjanovic, I. Milosevic, *Appl. Surf. Sci.* **2014**, *320*, 183–187.
- [26] R. A. Bepari, P. Bharali, B. K. Das, *J. Saudi Chem. Soc.* **2017**, *21*, S170–S178.
- [27] L. M. Cursaru, R. M. Piticescu, D. V. Dragut, I. A. Tudor, V. Kuncser, N. Iacob, F. Stoiciu, *Nanomaterials* **2020**, *10*, 85.
- [28] P. Mastrorilli, C. F. Nobile, G. Marchese, *Inorg. Chim. Acta* **1995**, *233*, 65–69.
- [29] J. D. Van Dyke, K. L. Kasperski, *J. Polym. Sci. Part A* **1993**, *31*, 1807–1823.
- [30] S. Özlem-Gundogdua, E. A. Gurelb, J. Hacaloglu, *J. Anal. Appl. Pyrolysis* **2015**, *113*, 529–538.
- [31] a) I. V. Chernyshova, M. F. Hochella, A. S. Madden, *Phys. Chem. Chem. Phys.* **2007**, *9*, 1736–1750; b) F. Wang, X. F. Qin, Y. F. Meng, Z. L. Guo, L. X. Yang, Y. F. Ming, *Mater. Sci. Semicond. Process.* **2013**, *16*, 802–806.
- [32] C. P. Marshall, W. J. B. Dufresne, C. J. Ruffledt, *J. Raman Spectrosc.* **2020**, *51*, 1522–1529.
- [33] a) L. L. A. de Faria, S. Venâncio Silva, M. T. de Oliveira, *J. Raman Spectrosc.* **1997**, *28*, 873–878; b) O. N. Shebanova, P. Lazor, *J. Solid State Chem.* **2003**, *174* (2), 424–430; c) M. Hanesch, *Geophys. J. Int.* **2009**, *177*, 941–948.
- [34] a) L. B. Modesto Lopez, J. D. Pasteris, P. Biswas, *Appl. Spectrosc.* **2009**, *63*, 627–635; b) D. Bersani, P. P. Lottici, A. Montenero, *J. Raman Spectrosc.* **1999**, *30*, 355–360.
- [35] B. Pal, M. Sharon, *Thin Solid Films* **2000**, *379*, 83–88.
- [36] Y. C. Zhang, J. Y. Tang, X. Y. Hu, *J. Alloys Compd.* **2008**, *462*, 24–28.
- [37] a) S. Sun, H. Zeng, *J. Am. Chem. Soc.* **2002**, *124*, 8204–8205; b) J. Wang, B. Zhang, L. Wang, M. Wang, F. Gao, *Mater. Sci. Eng. C* **2015**, *48*, 416–423; c) D. Maity, S. N. Kale, R. Kaul-Ghanekar, J.-M. Xue, J. Ding, *J. Magn. Mater.* **2009**, *321*, 3093–3098.
- [38] T. Yamashita, P. Hayes, *Appl. Surf. Sci.* **2008**, *254*, 2441–2449.
- [39] a) D. D. Hawn, B. M. DeKoven, *Surf. Interface Anal.* **1987**, *10*, 63–74; b) M. Muhler, R. Schlögl, G. Ertl, *J. Catal.* **1992**, *138*, 413–444.
- [40] S. Bandi, A. K. Srivastav, *Cryst. Growth Des.* **2021**, *21*, 16–22.
- [41] M. Ahmadzadeh, C. Romero, J. McCloy, *AIP Adv.* **2018**, *8*, 056807.
- [42] G. P. Guntlin, S. T. Ochsenbein, M. Wörle, R. Erni, K. V. Kravchyk, M. V. Kovalenko, *Chem. Mater.* **2018**, *30*, 1249–1256.
- [43] D. Formenti, F. Ferretti, F. K. Scharnagl, M. Beller, *Chem. Rev.* **2019**, *119*, 2611–2680.
- [44] a) D. Formenti, C. Topf, K. Junge, F. Ragaini, M. Beller, *Catal. Sci. Technol.* **2016**, *6*, 4473–4477; b) G. Romanazzi, V. Petrelli, A. M. Fiore, P. Mastrorilli, M. M. Dell’Anna, *Molecules* **2021**, *26*, 1120; c) R. Yun, L. Hong, W. Ma, W. Jia, S. Liu, B. Zheng, *ChemCatChem* **2019**, *11*, 724–728.
- [45] a) M. Tian, X. Cui, K. Liang, J. Ma, Z. Dong, *Inorg. Chem. Front.* **2016**, *3*, 1332–1340; b) I. T. Papadas, S. Fountoulaki, I. N. Lykakis, G. S. Armatas, *Chem. Eur. J.* **2016**, *22*, 4600–4607; c) R. V. Jagadeesh, K. Natte, H. Junge, M. Beller, *ACS Catal.* **2015**, *5*, 1526–1529; d) J. Lv, Z. Liu, Z. Dong, *J. Mol. Catal.* **2020**, *498*, 111249.
- [46] S. Xu, D. Yu, S. Liao, T. Ye, H. Sheng, *RSC Adv.* **2016**, *6*, 96431–96435.
- [47] H. Niu, J. Lu, J. Song, L. Pan, X. Zhang, L. Wang, J.-J. Zou, *Ind. Eng. Chem. Res.* **2016**, *55*, 8527–8533.
- [48] X. Cui, X. Zhou, Z. Dong, *Catal. Commun.* **2018**, *107*, 57–64.
- [49] M. M. Dell’Anna, G. Romanazzi, P. Mastrorilli, *Curr. Org. Chem.* **2013**, *17*, 1236–1273.
- [50] A. Rizzuti, M. C. Dipalo, I. Allegretta, R. Terzano, N. Cioffi, P. Mastrorilli, M. Mali, G. Romanazzi, A. Nacci, M. M. Dell’Anna, *Catalysts* **2020**, *10*, 1–23.
- [51] G. Romanazzi, A. M. Fiore, M. Mali, A. Rizzuti, C. Leonelli, A. Nacci, P. Mastrorilli, M. M. Dell’Anna, *J. Mol. Catal.* **2018**, *446*, 31–38.
- [52] W. Wu, W. Zhang, Y. Long, J. Qin, J. Ma, *J. Mol. Catal.* **2020**, *497*, 111226.
- [53] M. M. Dell’Anna, P. Mastrorilli, C. F. Nobile, G. P. Suranna, *J. Mol. Catal. A* **1995**, *105*, 17–22.

Manuscript received: November 2, 2021

Revised manuscript received: January 11, 2022

RESEARCH ARTICLE



Calcination of *Fe_POL* (a polymer supported Fe(III) complex) in air yields nanometric crystalline hematite

(*Hem_400_air*) which efficiently catalyzes transfer hydrogenation of nitroarenes.

Dr. A. M. Fiore, Dr. G. Varvaro, Dr. E. Agostinelli, Prof. A. Mangone, Prof. E. De Giglio, Prof. R. Terzano, Dr. I. Allegretta, Prof. M. M. Dell'Anna, Dr. S. Fiore*, Prof. P. Mastrorilli*

1 – 11

Synthesis and Use in Catalysis of Hematite Nanoparticles Obtained from a Polymer Supported Fe(III) Complex



Open Access